Received December 28, 2018, accepted January 10, 2019, date of publication January 22, 2019, date of current version February 8, 2019.

Digital Object Identifier 10.1109/ACCESS.2019.2894133

An Ultra-Wideband Reflective Phase Gradient Metasurface Using Pancharatnam-Berry Phase

BAOQIN LIN, (Member, IEEE), JIANXIN GUO, LINTAO LV, ZHE LIU, XIANG JI, AND JING WU
Xijing University, Xi'an, China

Corresponding author: Baoqin Lin (aflbq@sina.com)

This work was supported in part by the National Natural Science Foundation of China under Grant 61471387, in part by the Scientific Research Program Funded by the Shaanxi Provincial Education Department under Grant 18JK1195, and in part by the Key Research and Development Plan Project of Shaanxi Provincial Science and Technology Department under Grant 2018ZDXM-NY-014.

ABSTRACT Designing a transmissive and reflective phase gradient metasurface (PGM) using Pancharatnam–Berry (PB) geometrical phase must be based on an appropriate metasurface, which can realize circular-polarization (CP)-conversion transmission and CP-maintaining reflection, respectively. When an appropriate metasurface is proposed, a PGM can be easily constructed by gradually rotating the anisotropic or chiral resonators in different unit cells. In this paper, to design an ultra-wideband reflective PGM, first, an ultra-wideband CP-maintaining metasurface is proposed, and the numerical simulation results show that the proposed metasurface can realize CP-maintaining reflection at CP incidence between 8.43 and 26.93 GHz; in addition, a PB phase will be generated in its co-polarized reflection coefficient by rotating the anisotropic resonators in its unit cells. Thus, based on the metasurface, an ultra-wideband PGM is constructed successfully, the simulated and experimental results show that the PGM can realize ultra-wideband anomalous reflection at arbitrarily polarized incidence, and almost all the reflected waves at right-handed and left-handed CP (RHCP and LHCP) incidences will both be deflected to an anomalous direction; in addition, the reflected waves at linear and elliptical polarized (LP and EP) incidences will be separated into two beams for the LP and EP waves that can both be decomposed into a pair of RHCP and LHCP waves. Furthermore, finally, a detailed theoretical analysis is presented for the CP-maintaining reflection of the proposed metasurface.

INDEX TERMS Phase gradient, polarization-maintaining reflection, metasurface, circular polarization.

I. INTRODUCTION

Metasurfaces are two dimensional metamaterials with sub-wavelength thickness, which usually consist of a planar array of resonant unit cells mounted on a dielectric substrate. Through reasonable design of these resonant unit cells, all the basic properties of electromagnetic (EM) waves can be tailored by using various metasurfaces. In particular, when the resonators in different units have a regular variation, a phase gradient metasurface (PGM) will be constructed, which can be used to control the wave-front shape and introduce an additional parallel wave vector to redirect the reflected or refracted wave to a desired direction. Thus many extraordinary phenomena can be realized by various PGMs, such as anomalous reflection/refraction [1]–[11], negative refraction [1], [12], [13], surface wave conversion [14], [15], beam focusing [16]–[22], and vortex beam generation [23]–[30].

Attributed to the multi-functionalities of these PGMs, they have attracted considerable attention in recent years, and various kinds of PGMs have been proposed [1]–[30]. The key to designing a PGM is how to make a metasurface structure generate a phase gradient under an EM wave incidence. To generate a desired phase gradient in a metasurface structure, the following two methods are usually used: one is gradually changing the size and shape of the resonators in different unit cells to introduce an appropriate resonant phase difference between adjacent unit cells, the other one is gradually rotating the anisotropic or chiral resonators in different unit cells to introduce an appropriate geometrical phase difference between adjacent unit cells. In the first method, gradually changing the size and shape of the resonators in different unit cells can make the resonant frequency of each resonator different, thus let the array of resonators have space-variant phase response and generate a phase gradient under an EM wave incidence. This method is a common one, which can be used to design various PGMs, even about polarization-independent PGMs. The second method is to use a so-called Pancharatnam-Berry (PB) geometrical

phase [31], [32], which can be generated in cross-polarized transmission or co-polarized reflection coefficient at circular-polarized (CP) incidence by rotating the anisotropic or chiral resonator in the unit cell of a metasurface, thus based on an appropriate metasurface, which can realize CP-conversion transmission [33], [34] or CP-maintaining reflection [35] and make its cross-polarized transmission or co-polarized reflection coefficient approximate to 1.0 at CP incidence, a PGM can be designed by gradually rotating the anisotropic or chiral resonators in different unit cells. Now this method has been widely used to design various PGMs, a lot of PGMs have been proposed based on various appropriate metasurfaces. In particular, based on an ultra-wideband CP-conversion or CP-maintaining metasurface, the designed PGM can work within an ultra-wide band for the PB geometrical phase can theoretically be generated at any frequency and the working band of the designed PGM can keep the same with the original metasurface.

In this work, we propose an ultra-wideband CP-maintaining metasurface at first, which is an orthogonal anisotropic structure with a pair of symmetric axes u and v along $\pm 45°$ directions with respect to y-axis direction. The simulated results show that the metasurface can realize CP-maintaining reflection and keep the handedness of the reflected wave the same as that of the incident wave in the ultra-wideband frequency range from 8.43 GHz to 26.93 GHz, thus we have designed an ultra-wideband reflective PGM based on the proposed metasurface, the simulated and experimental results show that the PGM can realize ultra-wideband anomalous reflection at arbitrary polarized incidence, moreover, its working band can be kept the same as that of the original CP-maintaining metasurface (8.43-26.93GHz).

II. DESIGN AND SIMULATION

Designing a reflective PGM using PB phase must be based on a CP-maintaining metasurface. When the anisotropic or chiral resonators in the unit cells of a CP-maintaining metasurface are all rotated by an angle φ in a clockwise direction, the total reflected wave of the metasurface at right-handed and left-handed CP (RHCP and LHCP) incidences can be expressed as [36]:

$$\boldsymbol{E_r}|_{\mathrm{RHCP}} = r_{-+}E_i^+ + r_{++}e^{+j2\varphi}E_i^+, \tag{1a}$$

and

$$\boldsymbol{E}_r|_{\mathrm{LHCP}} = r_{+-}E_i^+ + r_{--}e^{-j2\varphi}E_i^-, \tag{1b}$$

respectively, wherein r_{-+}, r_{++}, r_{+-} and r_{--} are the cross- and co-polarized reflection coefficients of the initial metasurface at RHCP(+) and LHCP(−) incidences, it is shown that the phase of the total reflected wave at RHCP and LHCP incidences will be altered by $+2\varphi$ and -2φ respectively when the magnitudes of r_{++} and r_{--} are close to 1.0 and those of r_{-+} and r_{+-} are close to 0.0.

Equation (1) indicates that the key to designing a reflective PGM using PB phase is to design an appropriate

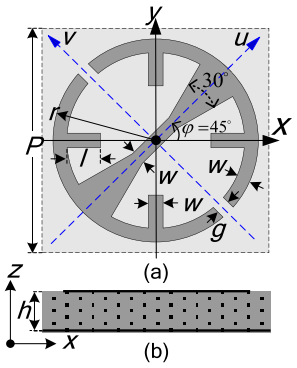

FIGURE 1. Unit cell of the proposed CP-maintaining metasurface: (a) Top view, (b) Side view.

CP-maintaining metasurface. When a CP-maintaining metasurface with appropriate unit structure is proposed, a PGM can be easily constructed by gradually rotating the anisotropic or chiral resonators in the different unit cells of the metasurface. In this work, we proposed an ultra-wideband CP-maintaining metasurface at first, which is comprised of a two-dimensional square array of anisotropic resonators mounted on a grounded dielectric substrate. One unit cell of the metasurface is shown in Fig. 1, it is shown that the anisotropic resonator in the unit cell is a circular structure, which is most suitable for rotation, in addition, it is an orthogonal anisotropic structure with a pair of symmetric axis u and v, which are perpendicular to each other, we define the rotation angle φ of the anisotropic resonator as the angle between the positive u-axis and positive x-axis, now the rotation angle φ is set to 45°. After appropriate selection, the geometrical parameters of the unit structure, which are shown in Fig. 1, are chosen as follows: $P = 6.00$ mm, $r = 2.60$ mm, $l = 1.00$ mm, $w = 0.20$ mm, $g = 1.50$ mm and $h = 3.00$mm; in addition, the metallic layer, together with the grounded plane, is modeled as a 0.017mm copper film with an electric conductivity $\sigma = 5.8 \times 10^7$S/m, and the dielectric substrate is selected as PTFE one with a relative permittivity of 1.8.

To numerically investigate the CP-maintaining reflection performance of the anisotropic metasurface, we have carried out numerical simulations to analyze its reflection behavior at CP incidence using Ansoft HFSS. When the input is successively set as a RHCP and LHCP waves, the simulated results, the cross- and co-polarized reflection coefficients, are shown in Figs. 2(a), in addition, the polarization maintaining ratios (PMRs), which are calculated by the equations $\mathrm{PMR} = |r_{++}|^2/(|r_{++}|^2 + |r_{-+}|^2)$ and $\mathrm{PMR} = |r_{--}|^2/(|r_{+-}|^2 + |r_{--}|^2)$ respectively, are shown in Fig. 2(b). In Fig. 2(a), it is indicated that the magnitudes of the cross- and co-polarized reflection coefficients at RHCP and LHCP incidences are almost completely the same, the magnitudes of r_{++} and r_{--} are close to 0dB and the magnitudes of r_{-+} and r_{+-} are much less than −10dB in the ultra-wideband frequency range from 8.43 GHz to 26.93 GHz; in addition, Fig.2 (b) shows that the PMRs at RHCP and LHCP incidences are both

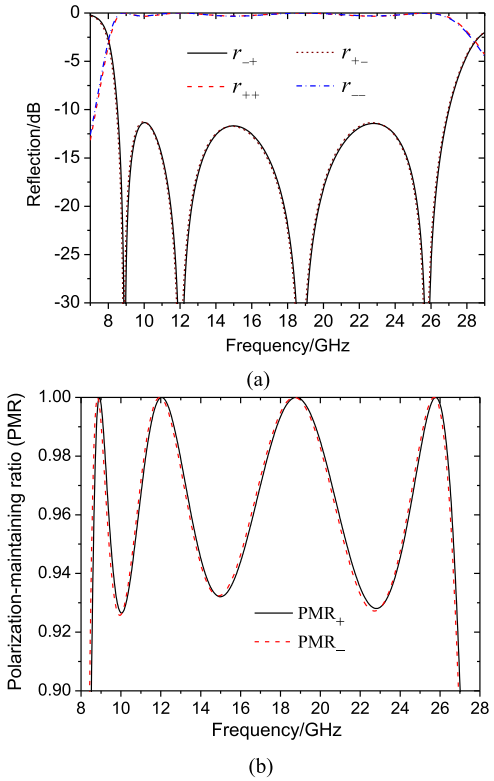

FIGURE 2. Simulated results of the proposed CP-maintaining metasurface at RHCP and LHCP incidences: (a) the magnitudes of the cross- and co-polarized reflection coefficients, (b) the polarization-maintaining ratios (PMRs).

much higher than 90% in this frequency range, which means that an ultra-wideband CP-maintaining reflection is realized by the metasurface in this band, its relative bandwidth is up to 104.6%.

In addition, in order to prove that PB phase will be generated in the co-polarized reflection coefficients r_{++} and r_{--} by rotating the anisotropic resonators in the unit cells of the proposed metasurface, we have simulated the metasurface many times at RHCP and LHCP incidences when the rotation angle φ of the anisotropic resonator in its unit cell was gradually increased by 30°. The simulated results, shown in Fig. 3(a) and (b), indicate that the phase of r_{++} gradually increases but the phase of r_{--} gradually decreases along with the increase of the rotation angle φ at the all frequencies, and they are both altered by almost 60° at each time, which implies that almost $2\Delta\varphi = 60°$ PB phase is generated at all frequencies when the rotation angle φ is increased by $\Delta\varphi = 30°$, and the PB phases generated at RHCP and LHCP incidences are $+2\Delta\varphi$ and $-2\Delta\varphi$, respectively. In addition, Fig. 3 (c) and (d) show that the phases of r_{-+} and r_{+-} always remain the same at all frequencies, it is indicated that no PB phase is generated in r_{-+} and r_{+-} and the phase of r_{-+} and r_{+-} can't be changed by rotating the anisotropic resonators.

According to the simulated results shown in Fig. 2 and 3, we proposed a PGM based on the proposed metasurface in succession. The super unit of the PGM is shown in Fig. 4, which consists of six sub-unit cells, the rotation angles φ of

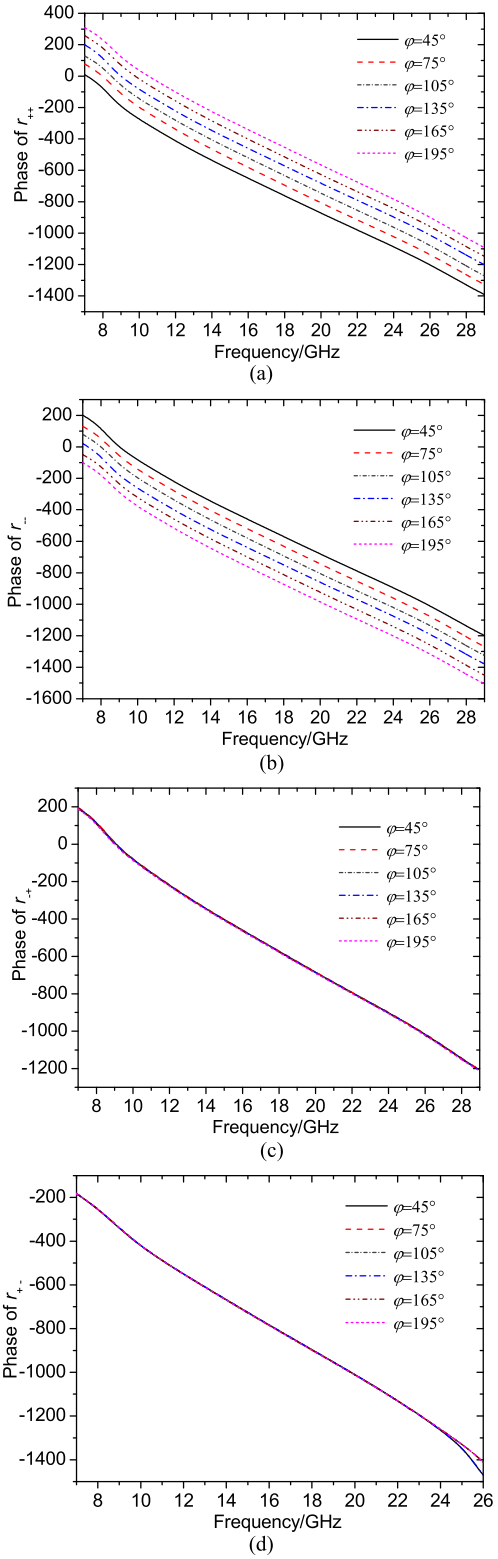

FIGURE 3. Simulated results of the CP-maintaining metasurface with different rotating angle φ: (a) the phase of r_{++}, (b) the phase of r_{--}, (c) the phase of r_{-+}, (d) the phase of r_{+-}.

the anisotropic resonators in the six sub-unit cells gradually increase from left to right, and the angle difference $\Delta\varphi$ in the adjacent units is just 30°. According to the simulation results

in Fig. 3, we can know that r_{++} and r_{--} in the super unit can realize a discrete phase-change from left to right at all frequencies, the phase-change step will be close to $\Delta\alpha = \pm 2\Delta\varphi = \pm 60°$ along each sub-unit cell, and $\pm 360°$ phase-change will be realized in total super unit, this means that a constant phase gradient will be generated in r_{++} and r_{--} at RHCP and LHCP incidences, which can be expressed as:

$$\nabla\alpha|_{\mathrm{RHCP}} = \frac{\Delta\alpha}{P} = \frac{2\Delta\varphi}{P} = \frac{2\pi}{L} \tag{2a}$$

and

$$\nabla\alpha|_{\mathrm{LHCP}} = \frac{\Delta\alpha}{P} = \frac{-2\Delta\varphi}{P} = \frac{-2\pi}{L}, \tag{2b}$$

respectively, wherein $L = 6P = 36.0$ mm is the period of super unit. Now it is indicated that the two phase gradients generated in r_{++} and r_{--} have the same amplitudes but are in opposite directions. Due to the generated phase gradient $\nabla\alpha$, the co-polarized reflected waves at RHCP and LHCP incidences will possess an additional parallel wave vector component $k_t = \nabla\alpha$ along the surface of the PGM, thus the co-polarized reflected waves will be deflected to an anomalous direction. According to the generalized Snell's law, the reflected angle of the co-polarized reflected waves can be calculated using the following equation:

$$\theta_r = \arcsin\left(\frac{k_0 \sin\theta_i + \nabla\alpha}{k_0}\right), \tag{3}$$

wherein k_0 is the wave-vector in free space and θ_i is the incident angle. In combination with Equation (2) and $k_0 = 2\pi/\lambda$, at normal incidence, Equation (3) can be simplified as:

$$\theta_r = \arcsin\left(\pm\lambda/L\right), \tag{4}$$

wherein '+' corresponds to RHCP incidence and '−' corresponds to LHCP incidence, it is indicated that the reflected angles of the co-polarized reflected wave at normal RHCP and LHCP incidences are equal in size but opposite in direction. In addition, about the cross-polarized reflected waves at RHCP and LHCP incidences, Fig. 3 shows that the phases of r_{-+} and r_{+-} can't be changed by rotating the anisotropic resonator in the unit cell of the metasurface, so the phases of r_{-+} and r_{+-} will keep the same at all sub-unit cells of the PGM, and the cross-polarized reflected wave will not be deflected to an anomalous direction, their reflection angles will remain equal to the incident angle, which means that the total reflected waves at RHCP and LHCP incidences will both be separated into two beams with different reflection angle. The simulated results shown in Fig. 2 indicate that the PMRs at RHCP and LHCP incidences are both much higher than 90% between 8.43 GHz to 26.93 GHz, which implies that the incident wave basically has all been converted to the co-polarized reflected wave, thus we can ignore the cross-polarized reflected beam, and consider that only the deflected co-polarized reflected beam exists at RHCP and LHCP incidences in 8.43-26.93 GHz. However, in other frequency bands, there are still the phase gradient $\nabla\alpha$ generated in r_{++} and r_{--}, but the deflected co-polarized reflected beam will be very small, thus it can be ignored, which just shows that the working band of the designed PGM can keep the same as that of the original CP-maintaining metasurface.

FIGURE 4. The super unit of the proposed PGM.

Furthermore, when the PGM is illuminated by a linear and elliptical polarized (LP and EP) waves, we can consider that it is illuminated by a pair of RHCP and LHCP waves simultaneously because arbitrary LP and EP waves can both be decomposed into a pair of RHCP and LHCP waves. In this way, we know that the reflected waves at LP and EP incidences will both be separated into two beams, which are just the two co-polarized reflected beams excited by the pair of RHCP and LHCP incident waves. At normal LP and EP incidences, the reflected angles of the two reflected beams will be equal in size but opposite in direction; moreover, at LP incidence, the two reflected beams will have the same amplitudes due to the decomposition of LP waves into LHCP and RHCP waves with equal amplitudes; however, the two reflected beams excited by EP incident wave will have different amplitudes.

In succession, we verified the above theoretical predictions by a series of numerical simulations. In these simulations, we assume that a finite size PGM (6 mm∗252 mm), which consists of seven super units in the same row, is irradiated by different polarized incident waves successively, the simulation structure is surrounded by a pair of periodic boundaries on the front and back sides and multiple radiation boundaries on the other sides. As the simulated results, the E-field distribution of the total reflected wave on a longitudinal section of the simulation structure is monitored to observe the anomalous reflection. Firstly, the incident wave is assumed as a normal RHCP one, the simulated results, shown in Fig. 5(a), (b), (c), (d) and (e), indicate that almost all of the reflected wave has been deflected to an anomalous direction at different frequencies, the reflected angles at 9.0, 12.0, 15.0, 20.0 and 25.0 GHz are almost 68°, 44°, 34°, 25° and 20° respectively, which agree well with the theoretically predicted values 67.8°, 44.0°, 33.7°, 24.6° and 19.5° [$\theta_r = \arcsin\left(\lambda/L\right)$], it is verified that an effective PGM has been successfully designed based on the proposed metasurface. Secondly, we assume that the PGM is irradiated by a normal LP wave, the simulated results are shown in Fig. 5(f) and (g), it is indicated that the reflected wave at the LP incidence has all been separated into two beams at the frequencies 9.0 and 15.0 GHz, moreover, the amplitudes of the two beams are almost the same. Finally, the incident wave is assumed as a right-handed EP (RHEP) wave, whose polarization ratio is 3.0 and the polarization angle is 90°, thus it can be decomposed into a pair of RHCP and LHCP waves with an amplitude ratio 2:1. The simulated results in Fig. 5(h) indicate that its reflected wave has also been separated into two beams at

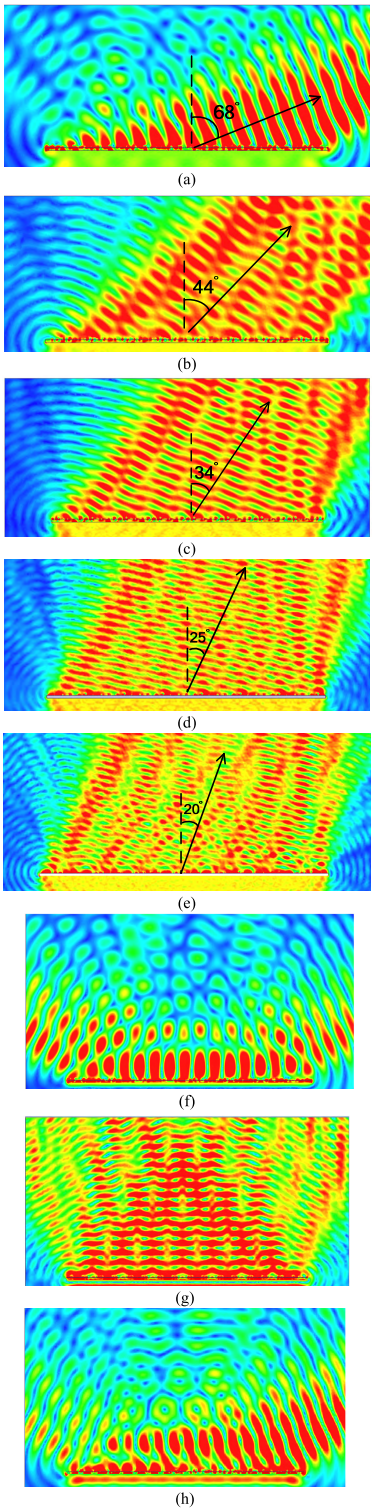

FIGURE 5. Simulated results of the proposed PGM at different incidences: E-electric field distributions at normal RHCP incidence at 9.0 GHz (a), 12.0 GHz (b),15.0 GHz (c), 20.0 GHz (d) and 25.0 GHz (e); E-electric field distributions at normal LP incidence at 9.0 GHz (f) and 15.0 GHz (g); E-electric field distribution at normal RHEP incidence at 9.0 GHz (h).

the frequencies 9.0 GHz, in addition, the amplitude ratio of the two beams is almost equal to 2:1. According to all the simulated results in Fig. 5, we can announce that the PGM can realize wideband anomalous reflection at arbitrary polarized incidence, which agree well with the theoretical predictions.

III. THEORY ANALYSIS

The key to designing a PGM using PB phase is to design an appropriate metasurface, how to design a CP-maintaining metasurface? Why the proposed metasurface shown in Fig.1 can realize CP-maintaining reflection, we present a detailed analysis for it. The proposed metasurface is an orthogonal anisotropic structure with a pair of symmetric axes u and v, which are perpendicular to each other. At u- and v-polarized incidences, no cross-polarized reflected components will exist due to the symmetry, therefore, in the U-V coordinate system, the reflection matrix $\mathbf{R}_{\text{lin}}$ for LP incidence can be expressed as:

$$\begin{pmatrix} E_u^r \\ E_v^r \end{pmatrix} = \begin{pmatrix} r_{uu} & 0 \\ 0 & r_{vv} \end{pmatrix} \begin{pmatrix} E_u^i \\ E_v^i \end{pmatrix} = \mathbf{R}_{\text{lin}} \begin{pmatrix} E_u^i \\ E_v^i \end{pmatrix}, \tag{5}$$

wherein the co-polarized reflection coefficients r_{uu} and r_{vv} are mutually independent due to the anisotropy, but the magnitudes of r_{uu} and r_{vv} are both very close to 1.0 because of the little dielectric loss. So if we neglect the dielectric loss, one equation can be established as follow:

$$r_{vv} = r_{uu} e^{-j\Delta\psi}, \tag{6}$$

wherein $\Delta\psi$ denotes the phase difference between r_{uu} and r_{vv}.

For a CP wave consists of two perpendicular LP components with equal amplitude and $\pm 90°$ phase difference, the reflection matrix $\mathbf{R}_{\text{cir}}$ for CP incidence can be derived from $\mathbf{R}_{\text{lin}}$ in Equation (5). In Fig. 1, it is shown that the incident wave is in -Z axis direction, and the reflected wave is +Z axis, so the incident RHCP unit wave, together with the reflected LHCP unit wave, can be expressed as $\hat{e} = \hat{e}_u + i\hat{e}_v$, and the reflected RHCP and incident LHCP unit wave can both be expressed as $\hat{e} = \hat{e}_u - i\hat{e}_v$. When the incident wave is supposed as a RHCP unit wave $\boldsymbol{E}^i = \hat{e}_x + i\hat{e}_y$, according to Equation (5), the total reflected wave can be obtained and expressed as:

$$\begin{aligned} \boldsymbol{E}^r &= E_u^r \hat{e}_u + E_v^r \hat{e}_v = r_{uu}\hat{e}_u + i r_{vv}\hat{e}_v \\ &= \frac{r_{uu} - r_{vv}}{2}(\hat{e}_u - i\hat{e}_v) + \frac{r_{uu} + r_{vv}}{2}(\hat{e}_u + i\hat{e}_v), \end{aligned} \tag{7}$$

which means that the co- and cross-polarized reflection coefficients at RHCP incidence can be expressed as:

$$\begin{aligned} r_{++} &= \frac{1}{2}(r_{uu} - r_{vv}) = \frac{1}{2} r_{uu}\left(1 - e^{-j\Delta\psi}\right) \\ r_{-+} &= \frac{1}{2}(r_{uu} + r_{vv}) = \frac{1}{2} r_{uu}\left(1 + e^{-j\Delta\psi}\right). \end{aligned} \tag{8}$$

In addition, a similar deduction is performed at LHCP incidence, the total reflection matrix $\mathbf{R}_{\text{cir}}$ for CP wave is obtained as follow:

$$\mathbf{R}_{cir} = \begin{pmatrix} r_{++} & r_{+-} \\ r_{-+} & r_{--} \end{pmatrix} = \frac{1}{2} \begin{pmatrix} r_{uu} - r_{vv} & r_{uu} + r_{vv} \\ r_{uu} + r_{vv} & r_{uu} - r_{vv} \end{pmatrix}$$

$$= \frac{1}{2} r_{uu} \begin{pmatrix} 1 - e^{-j\Delta\psi} & 1 + e^{-j\Delta\psi} \\ 1 + e^{-j\Delta\psi} & 1 - e^{-j\Delta\psi} \end{pmatrix}. \quad (9)$$

Thus the magnitudes of r_{++}, r_{--}, and r_{-+}, r_{+-} can be expressed by using the following equation:

$$\begin{aligned} |r_{++}| = |r_{--}| &= \frac{1}{2} |r_{uu}| \left| 1 - e^{-j\Delta\psi} \right| \\ &= \frac{1}{2} |1 - \cos(\Delta\psi) + j \sin(\Delta\psi)| \\ &= \sqrt{(1 - \cos\Delta\psi)/2} \quad (10a) \\ |r_{-+}| = |r_{+-}| &= \frac{1}{2} |r_{uu}| \left| 1 + e^{-j\Delta\psi} \right| \\ &= \frac{1}{2} |1 + \cos(\Delta\psi) - j \sin(\Delta\psi)| \\ &= \sqrt{(1 + \cos\Delta\psi)/2}. \quad (10b) \end{aligned}$$

According to Equation (10), we can know that the orthogonal anisotropy of the metasurface structure, which results in the two independent reflection coefficients r_{uu} and r_{vv}, is the root cause of the CP-maintaining reflection, and the polarization state of the reflected wave can be completely determined by the phase difference $\Delta\psi$ between r_{uu} and r_{vv}. If the anisotropy of the metasurface structure is appropriate, multiple different eigenmodes will be excited by v- and u-polarized incidences, thus a large phase differences $|\Delta\psi|$ will be introduced in a wide frequency range. When $|\Delta\psi|$ is close to the maximum value 180° in a wide frequency band, the CP-maintaining reflection can be realized in the wide band. Why the CP-maintaining reflection can be realized when $|\Delta\psi|$ is close to 180°? In fact, if $|\Delta\psi| = 180°$, then $r_{vv} = r_{uu}e^{-j\Delta\psi} = -r_{uu}$, thus when the incident wave is assumed as a RHCP unit wave $\boldsymbol{E}^i = \hat{e}_u + i\hat{e}_v$, the reflected wave can be obtained as follow:

$$\boldsymbol{E}^r = E_u^r \hat{e}_u + E_v^r \hat{e}_v = r_{uu}\hat{e}_u + i r_{vv}\hat{e}_v = r_{uu}(\hat{e}_u - i\hat{e}_v), \quad (11)$$

which indicates the perfect CP-maintaining reflection is realized when $|\Delta\psi| = 180°$ because $\boldsymbol{E}^r = \hat{e}_u - i\hat{e}_v$ is just the expression formula of the reflected RHCP unit wave and the magnitude of r_{uu} is equal to 1.0 when the dielectric loss is neglected.

To illustrate the mechanization of the ultra-wideband CP-maintaining reflection in the proposed metasurface using Equation (10), we have carried out numerical simulations at u- and v-polarized incidences, respectively. The simulated results in Fig. 6(a) indicate that the phase difference $\Delta\psi$ between r_{uu} and r_{vv} is close to 180° in the ultra-wideband frequency range from 8.5 GHz to 26.9 GHz. In addition, Fig. 6(b) shows the magnitudes of r_{uu} and r_{vv} are both close to 1.0 at all frequencies, however, through detailed observation, it is found that the data curves of r_{uu} and r_{vv} have two minimum values at the frequencies 11.94 GHz, 27.92 GHz and 8.42 GHz, 20.26 GHz, respectively, which indicates that two pairs of different eigenmodes are excited in turn at the four different eigen-frequencies by u- and v-polarized incidences respectively, it is implied that it is just the two pairs of eigenmodes causing a large phase differences $\Delta\psi$ between r_{uu} and r_{vv} in the ultra-wideband frequency range. Finally, we have calculated the magnitudes of r_{-+} and r_{+-} using Equation (10b) according to the phase differences $\Delta\psi$ in Fig. 6(a), the calculated results are shown in Fig. 6(c), it is indicated that the calculated results are in good agreement with the simulated results in Fig. 2(a).

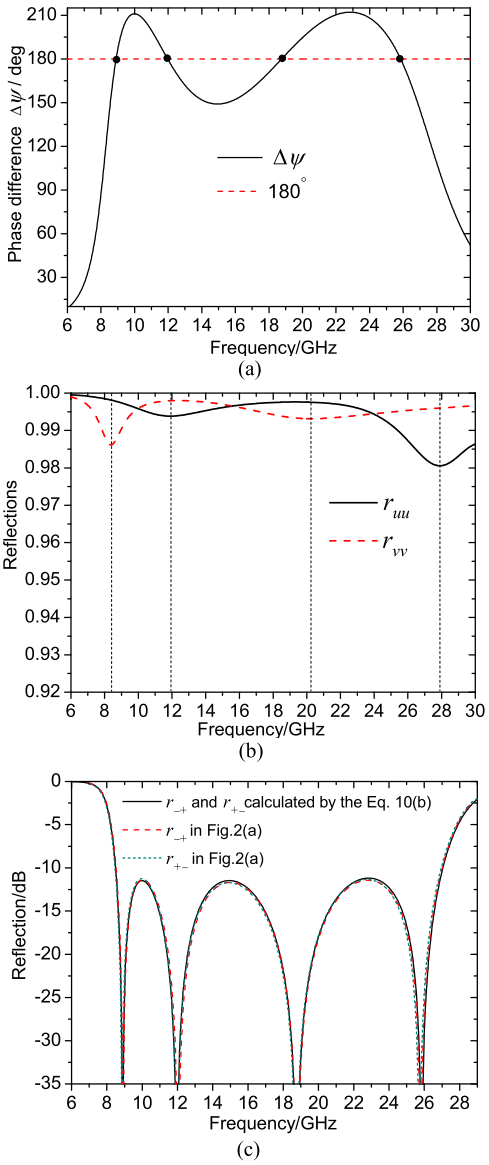

FIGURE 6. Simulated results of the proposed CP-maintaining metasurface at u- and v-polarized incidences: (a) the magnitudes of r_{uu} and r_{vv}, (b) the phase difference between r_{uu} and r_{vv}, (c) the comparison between the simulated and calculated r_{-+} and r_{-+}.

According to the above analyses, we can conclude that the orthogonal anisotropy of the metasurface structure is the root cause of the CP-maintaining reflection, all orthogonal anisotropic metasurfaces can realize CP-maintaining reflection when the phase difference $\Delta\psi$ between r_{uu} and r_{vv} is close to ±180°. In fact, in literature [37], it has been illustrated that an orthogonal anisotropic metasurfaces can also realize perfect linear-polarization-conversion when the phase difference $\Delta\psi$ is close to ±180°. If the metasurface structure

is in a X-Y coordinate system and the rotation angle φ is equal to 45°, as shown in Fig. 1(a), the magnitudes of the reflection coefficients at x- and y-polarized incidences can also be expressed as:

$$|r_{yx}| = |r_{xy}| = \sqrt{(1-\cos\Delta\psi)/2}$$
$$|r_{xx}| = |r_{yy}| = \sqrt{(1+\cos\Delta\psi)/2}. \quad (12)$$

According to Formula (10) and (12), we can know that this kind of orthogonal anisotropic metasurfaces can realize not only linear-polarization-conversion at LP incidence but also CP-maintaining reflection at CP incidence, moreover, $|r_{++}| = |r_{--}| = |r_{xy}| = |r_{yx}|$ and $|r_{-+}| = |r_{+-}| = |r_{yy}| = |r_{xx}|$. In recent years, a number of ultra-wideband reflective orthogonal anisotropic linear-polarization-conversion metasurfaces have been proposed in some literatures [37]–[45], however, in these literatures, only the linear-polarization-conversion performance has been concerned. Now we announce that these linear-polarization-conversion metasurfaces can all realize CP-maintaining reflection at CP incidences at the same time, moreover, they can be used to the design of PGM if the anisotropic resonator in the unit cell is suitable for rotating.

IV. EXPERIMENTAL RESULTS

Finally, in order to realize an experimental validation for our design, a laboratory sample was fabricated using standard print circuit board (PCB) technique, which consists of 45×45 unit cells with an area of 270mm×270mm as shown in Fig. 7(a). Firstly, we have measured its co-polarized scattering pattern at CP incidence by the method of measuring antenna pattern, the schematic illustration of our measurement setup is shown in Fig. 7(b), in which the laboratory sample is erected with these super units in horizontal direction, and two pairs of identical RHCP horn antennas are used, the transmitting antenna is fixed to emit a normal RHCP incident wave onto the laboratory sample, but the receiving antenna rotates around the laboratory sample in a horizontal plane to measure the co-polarized scattering pattern and find the maximum reflection direction at different frequencies. By using the two pairs of RHCP horn antennas with a continuous frequency doubling in working band (8-18GHz, 18-40GHz), the co-polarized scattering pattern was measured at the five frequencies 9.0, 12.0, 15.0, 20.0 and 25.0 GHz. The measured results are shown in Fig. 7(c), it is indicated that the maximum scattering directions at the five frequencies are almost 66°, 44°, 34°, 25° and 20°, respectively, which agree well with the theoretically calculated results: 67.8°, 44.0°, 33.7°, 24.6° and 19.5°; the second maximum scattering directions are all in 180° direction, and a strong forward scattering exists at each frequency, this is mainly because the size of the laboratory sample is very limited, although the transmitting antenna is not far from the laboratory sample, there is still a part of incident wave that has not been reflected by it; in addition, a back scattering also exists at each frequency, which is just the cross-polarized reflected wave for the reflection angle

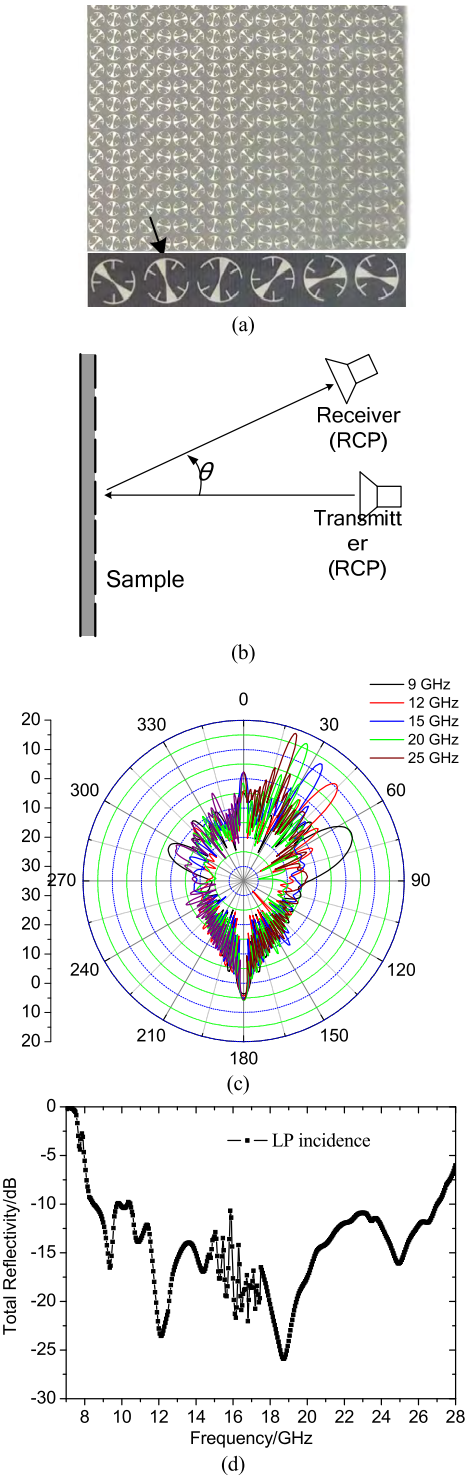

FIGURE 7. Photographs of the fabricated PGM sample (a), the schematic of the measurement setup (b) and the measured results: the scattering pattern at normal RHCP incidence (c) and the total reflectivity at normal LP incidence (d).

of the cross-polarized reflected wave remains equal to the incident angle; furthermore, the size of the laboratory sample is limited, which can be equivalent to a finite antenna array, thus many big side lobes can be seen at each case. Finally, the total reflectivity R_{total} of the laboratory sample at normal

LP wave incidence was measured in the ultra-wideband frequency range from 7.5 GHz to 28.0 GHz. In the measurement, the used measurement setup was basically the same as the one shown in Fig. 7(b), except that the two pairs of RHCP horn antennas were replaced by a pair of LP horn antennas and the angle θ between the two antennas was fixed at 4.0°. The co- and cross-polarized reflection coefficients were measured successively when the receiving LP horn antenna rotated by 0° and 90°, respectively, such the total reflectivity was obtained by the equation $R_{total} = |r_{yy}|^2 + |r_{xy}|^2$. The measured results, shown in Fig. 7(d), indicate that the total reflectivity is significantly decreased between 8.5 GHz to 26.8 GHz, which just proves that the anomalous reflection occurs simultaneously under LP incidence in the ultra-wideband frequency range from 8.5 GHz to 26.8 GHz.

V. CONCLUSION

This work presents the design of an ultra-wideband reflective PGM using PB phase. In the design process, an ultra-wideband CP-maintaining metasurface is proposed firstly. Numerical simulations show that the metasurface can realize CP-maintaining reflection at CP incidence in the frequency range from 8.43 GHz to 26.93 GHz; in addition, a PB phase can be generated in its co-polarized reflection coefficients r_{++} and r_{--} at all frequencies by rotating the anisotropic resonators in its unit cells. Thus an ultra-wideband PGM is easily proposed based on the CP-maintaining metasurface, the simulation and experimental results show that the proposed PGM can deflect the reflected wave to an anomalous direction at CP incidence, and the reflected waves at LP and EP incidences can be separated into two beams; in addition, the working band of the PGM is kept the same as that of the original CP-maintaining metasurface (8.43-26.93GHz), its relative bandwidth reaches 104.6%, such it is of great application values in RCS reduction, stealth surfaces, etc. Finally, through a detailed theoretical analysis, the root cause of the CP-maintaining reflection in the proposed metasurface is presented, moreover, it is found that previously proposed various reflective orthogonal anisotropic linear-polarization-conversion metasurfaces can all realize CP-maintaining reflection at CP incidences at the same time, they can all be used to the design of PGM if the anisotropic resonators in their unit cells are suitable for rotating.

REFERENCES

[1] N. Yu *et al.*, "Light propagation with phase discontinuities: Generalized laws of reflection and refraction," *Science*, vol. 334, no. 6054, pp. 333–337, Oct. 2011.
[2] F. Aieta, P. Genevet, N. Yu, M. A. Kats, Z. Gaburro, and F. Capasso, "Out-of-plane reflection and refraction of light by anisotropic optical antenna metasurfaces with phase discontinuities," *Nano Lett.*, vol. 12, no. 3, pp. 1702–1706, 2012.
[3] L. Huang *et al.*, "Dispersionless phase discontinuities for controlling light propagation," *Nano Lett.*, vol. 12, no. 11, pp. 5750–5755, 2012.
[4] X. Ni, N. K. Emani, A. V. Kildishev, A. Boltasseva, and V. M. Shalaev, "Broadband light bending with plasmonic nanoantennas," *Science*, vol. 335, no. 6067, p. 427, Jan. 2012.
[5] N. K. Grady *et al.*, "Terahertz metamaterials for linear polarization conversion and anomalous refraction," *Science*, vol. 340, no. 6138, pp. 1304–1307, 2013.
[6] C. Pfeiffer and A. Grbic, "Metamaterial Huygens' surfaces: Tailoring wave fronts with reflectionless sheets," *Phys. Rev. Lett.*, vol. 110, no. 19, p. 197401, May 2013.
[7] A. Pors and S. I. Bozhevolnyi, "Plasmonic metasurfaces for efficient phase control in reflection," *Opt. Express*, vol. 21, no. 22, pp. 27438–27451, 2013.
[8] J. Neu, R. Beigang, and M. Rahm, "Metamaterial-based gradient index beam steerers for terahertz radiation," *Appl. Phys. Lett.*, vol. 103, no. 4, p. 041109, 2013.
[9] K. Wang, J. Zhao, Q. Cheng, D. S. Dong, and T. J. Cui, "Broadband and broad-angle low-scattering metasurface based on hybrid optimization algorithm," *Sci. Rep.*, vol. 4, Aug. 2014, Art. no. 5935.
[10] H.-X. Xu, G.-M. Wang, T. Cai, J. Xiao, and Y.-Q. Zhuang, "Tunable Pancharatnam–Berry metasurface for dynamical and high-efficiency anomalous reflection," *Opt. Express*, vol. 24, no. 24, pp. 27836–27848, 2016.
[11] Y. Zhuang, G. Wang, J. Liang, T. Cai, W. Guo, and Q. Zhang, "Flexible and polarization-controllable diffusion metasurface with optical transparency," *J. Phys. D, Appl. Phys.*, vol. 50, no. 46, p. 465102, 2017.
[12] R. E. Christiansen and O. Sigmund, "Designing meta material slabs exhibiting negative refraction using topology optimization," *Structural Multidisciplinary Optim.*, vol. 54, no. 3, pp. 469–482, 2016.
[13] T. Suzuki and S. Kondoh, "Negative refractive index metasurface in the 2.0-THz band," *Opt. Mater. Express*, vol. 8, no. 7, pp. 1916–1925, 2018.
[14] S. Sun, Q. He, S. Xiao, Q. Xu, X. Li, and L. Zhou, "Gradient-index metasurfaces as a bridge linking propagating waves and surface waves," *Nature Mater.*, vol. 11, no. 5, pp. 426–431, 2012.
[15] H. Shi *et al.*, "Gradient metasurface with both polarization-controlled directional surface wave coupling and anomalous reflection," *IEEE Antennas Wireless Propag. Lett.*, vol. 14, pp. 104–107, 2014.
[16] X. Li, S. Xiao, B. Cai, Q. He, T. J. Cui, and L. Zhou, "Flat metasurfaces to focus electromagnetic waves in reflection geometry," *Opt. Lett.*, vol. 37, no. 23, pp. 4940–4942, 2012.
[17] A. Pors, M. G. Nielsen, R. L. Eriksen, and S. I. Bozhevolnyi, "Broadband focusing flat mirrors based on plasmonic gradient metasurfaces," *Nano Lett.*, vol. 13, no. 2, pp. 829–834, 2013.
[18] S. Wang, J. Lai, C. Chen, J. Sun, and T. Wu, "Wide-band achromatic flat focusing lens based on all-dielectric subwavelength metasurface," *Opt. Express*, vol. 25, no. 6, pp. 7121–7130, 2017.
[19] H. Li, G. Wang, J. Liang, X. Gao, H. Hou, and X. Jia, "Single-layer focusing gradient metasurface for ultrathin planar lens antenna application," *IEEE Trans. Antennas Propag.*, vol. 65, no. 3, pp. 1452–1457, Mar. 2017.
[20] Q. Fan, P. Huo, Y. Liang, F. Yan, T. Xu, and D. Wang, "Visible light focusing flat lenses based on hybrid dielectric-metal metasurface reflector-arrays," *Sci. Rep.*, vol. 7, Mar. 2017, Art. no. 45044.
[21] A. Boubakri, F. Choubeni, J. David, and T. H. Vuong, "A near zero refractive index metalens to focus electromagnetic waves with phase compensation metasurface," *Opt. Mater.*, vol. 69, pp. 432–436, Jul. 2017.
[22] H. Yi, S. W. Qu, B. J. Chen, X. Bai, K. B. Ng, and C. H. Chan, "Flat terahertz reflective focusing metasurface with scanning ability," *Sci. Rep.*, vol. 7, no. 1, 2017, Art. no. 3478.
[23] H. Chen, J. Hao, B.-F. Zhang, J. Xu, J. Ding, and H.-T. Wang, "Generation of vector beam with space-variant distribution of both polarization and phase," *Opt. Lett.*, vol. 36, no. 16, pp. 3179–3181, 2011.
[24] C. Pfeiffer and A. Grbic, "Controlling vector Bessel beams with metasurfaces," *Phys. Rev. Appl.*, vol. 2, no. 4, p. 044012, 2014.
[25] X. Yi *et al.*, "Generation of cylindrical vector vortex beams by two cascaded metasurfaces," *Opt. Express*, vol. 22, no. 14, pp. 17207–17215, 2014.
[26] X. Ma, "A planar chiral meta-surface for optical vortex generation and focusing," *Sci. Rep.*, vol. 5, May 2015, Art. no. 10365.
[27] B. Xu, C. Wu, and Z. Wei, "Generating an orbital-angular-momentum beam with a metasurface of gradient reflective phase," *Opt. Mater. Express*, vol. 6, no. 12, pp. 3940–3945, 2016.
[28] K. Zhang *et al.*, "Phase-engineered metalenses to generate converging and non-diffractive vortex beam carrying orbital angular momentum in microwave region," *Opt. Express*, vol. 26, no. 2, pp. 1351–1360, 2018.
[29] C. Fang *et al.*, "Broadband and high-efficiency vortex beam generator based on a hybrid helix array," *Opt. Lett.*, vol. 43, no. 7, pp. 1538–1541, 2018.
[30] Y. Ran, J. Liang, H. Li, and T. Cai, "High-performance broadband vortex beam generator using reflective Pancharatnam–Berry metasurface," *Opt. Commun.*, vol. 427, pp. 101–106, Nov. 2018.

[31] S. Pancharatnam, "Generalized theory of interference, and its applications," *Proc. Indian Acad. Sci.-A*, vol. 44, no. 5, pp. 247–262, 1956.
[32] M. V. Berry, "Quantal phase factors accompanying adiabatic changes," *Proc. Roy. Soc. London A, Math. Phys. Sci.*, vol. 392, no. 1802, pp. 45–57, 1996.
[33] L. Wu *et al.*, "Giant asymmetric transmission of circular polarization in layer-by-layer chiral metamaterials," *Appl. Phys. Lett.*, vol. 103, no. 2, p. 021903, 2013.
[34] S.-Y. Wang, W. Liu, and W. Geyi, "A circular polarization converter based on in-linked loop antenna frequency selective surface," *Appl. Phys. B*, vol. 124, no. 6, p. 126, 2018.
[35] Y.-F. Li *et al.*, "Wide-band circular polarization-keeping reflection mediated by metasurface," *Chin. Phys. B.*, vol. 24, no. 1, pp. 258–264, 2015.
[36] H.-T. Chen, A. J. Taylor, and N. Yu, "A review of metasurfaces: Physics and applications," *Rep. Prog. Phys.*, vol. 79, no. 7, p. 076401, 2016.
[37] B. Lin *et al.*, "Dual-band high-efficiency polarization converter using an anisotropic metasurface," *J. Appl. Phys.*, vol. 119, no. 18, p. 205428, 2016.
[38] H. Chen *et al.*, "Ultra-wideband polarization conversion metasurfaces based on multiple plasmon resonances," *J. Appl. Phys.*, vol. 115, no. 15, p. 177403, 2014.
[39] X. Gao, X. Han, H. O. Li, H. F. Ma, T. J. Cui, and W.-P. Cao, "Ultrawideband and high-efficiency linear polarization converter based on double V-shaped metasurface," *IEEE Trans. Antennas Propag.*, vol. 63, no. 8, pp. 3522–3530, Aug. 2015.
[40] S. Sui *et al.*, "Symmetry-based coding method and synthesis topology optimization design of ultra-wideband polarization conversion metasurfaces," *Appl. Phys. Lett.*, vol. 109, no. 1, p. 063908, 2016.
[41] B. Q. Lin, X. Y. Da, J. L. Wu, W. Li, Y. W. Fang, and Z. H. Zhu, "Ultra-wideband and high-efficiency cross polarization converter based on anisotropic metasurface," *Miceow. Opt. Tech. Lett.*, vol. 58, no. 10, pp. 2402–2405, Oct. 2016.
[42] J. L. Wu, B.-Q. Lin, and X.-Y. Da, "Ultra-wideband reflective polarization converter based on anisotropic metasurface," *Chin. Phys. B*, vol. 25, no. 8, p. 088101, 2016.
[43] M. I. Khan, Q. Fraz, and F. A. Tahir, "Ultra-wideband cross polarization conversion metasurface insensitive to incidence angle," *J. Appl. Phys.*, vol. 121, no. 4, p. 045103, 2017.
[44] H. Sun, C. Gu, X. Chen, Z. Li, L. Liu, and F. Martín, "Ultra-wideband and broad-angle linear polarization conversion metasurface," *J. Appl. Phys.*, vol. 121, no. 17, p. 174902, 2017.
[45] P. Xu, S.-Y. Wang, and W. Geyi, "A linear polarization converter with near unity efficiency in microwave regime," *J. Appl. Phys.*, vol. 121, no. 14, p. 144502, 2017.

BAOQIN LIN received the M.Sc. degree in electromagnetic field and microwave technology from Air Force Engineering University, Xi'an, China, in 2002, and the Ph.D. degree in electronic science and technology from the National University of Defense Technology, Changsha, China, in 2006. He is currently an Associate Professor with the Department of Information Engineering, Xijing University, Xi'an. His current research interests include metasurface for various applications, such as polarization conversion, coupling suppression, and RCS reduction, phased array antennas, and ultra-wideband antennas. He is a member of the IEEE Antennas and Propagation Society.

JIANXIN GUO received the M.Sc. degree in information and communications engineering from Air Force Engineering University, Xi'an, China, in 2000, and the Ph.D. degree in information and communications engineering from PLA Information Engineering University, Zhengzhou, China, in 2004. He is currently a Professor with the Department of Information Engineering, Xijing University, Xi'an. His current research interests include cognitive radio technologies, MIMO-OFDM wireless communications, and their implementation in GNU radio.

LINTAO LV received the M.Sc. degree in computer science and technology from Xi'an Jiaotong University, Xi'an, China, in 1982. He is currently a Full Professor and a Doctoral Advisor with the Department of Information Engineering, Xijing University, Xi'an. He has published over 90 scientific journals and international conference papers. His current research interests include artificial intelligence in big data, intelligent information processing, biological information security, pattern recognition, and cyber analysis and security.

ZHE LIU received the Ph.D. degree in control engineering and science from Xi'an Jiaotong University, Xi'an, China, in 2009. He is currently a Professor with the Department of Information Engineering, Xijing University, Xi'an. His current research interests include artificial intelligence, intelligent agriculture, and machine vision.

XIANG JI received the Ph.D. degree in signal and information process and technology from the Beijing University of Post and Telecommunication, Beijing, China, in 1998. He is currently an Associate Professor with the Department of Information Engineering, Xijing University, Xi'an, China. His current research interest includes radio communication technology, such as multiuser detection, interference suppression, synchronization method, and signal detection for Wi-Fi communication system. He is a member of the IEEE Spectrum.

JING WU received the B.S. degree in mathematics and applied mathematics from Yulin College, Yulin, China, in 2008. She is currently a Lecturer with Xijing University, Xi'an, China. Her current research interests include linear algebra, wavelets and filter banks, applied mathematics, and engineering mathematics.